Acta Astronautica ▮ (▮▮▮▮) ▮▮▮–▮▮▮

Contents lists available at SciVerse ScienceDirect

Acta Astronautica

journal homepage: www.elsevier.com/locate/actaastro

A graphical approach to electric sail mission design with radial thrust

Giovanni Mengali*, Alessandro A. Quarta, Generoso Aliasi

Dipartimento di Ingegneria Aerospaziale, University of Pisa, I-56122 Pisa, Italy

ARTICLE INFO

Article history:
Received 23 November 2011
Received in revised form
21 March 2012
Accepted 27 March 2012

Keywords:
Electric sail
Radial thrust
Potential well

ABSTRACT

This paper describes a semi-analytical approach to electric sail mission analysis under the assumption that the spacecraft experiences a purely radial, outward, propulsive acceleration. The problem is tackled by means of the potential well concept, a very effective idea that was originally introduced by Prussing and Coverstone in 1998. Unlike a classical procedure that requires the numerical integration of the equations of motion, the proposed method provides an estimate of the main spacecraft trajectory parameters, as its maximum and minimum attainable distance from the Sun, with the simple use of analytical relationships and elementary graphs. A number of mission scenarios clearly show the effectiveness of the proposed approach. In particular, when the spacecraft parking orbit is either circular or elliptic it is possible to find the optimal performances required to reach an escape condition or a given distance from the Sun. Another example is given by the optimal strategy required to reach a heliocentric Keplerian orbit of prescribed orbital period. Finally the graphical approach is applied to the preliminary design of a nodal mission towards a Near Earth Asteroid.

© 2012 Elsevier Ltd. All rights reserved.

1. Introduction

Due to their long flight times, space missions with low-thrust propulsion systems are usually studied in an optimal framework, by maximizing (or minimizing) a suitable scalar performance index. The latter coincides, for example, with the propellant mass for electrical propulsion systems [1,2] or with the total flight time for a propellantless thruster as a solar sail [3,4] or an electric sail [5–10]. The solution of the optimal control problem associated to the design of the space trajectory is the output of a complex numerical optimization process, and the solution is typically found using a dedicated software. Only in a few cases the optimal control problem can be fully solved in an analytical or graphical form. One of such special cases is represented by the problem of calculating the optimal escape conditions for a space vehicle with constant, outward, propulsive acceleration. The first solution to this problem was analytically found by Tsien [11] assuming that the spacecraft is placed on a parking circular orbit and, recently, was extended by Mengali and Quarta [12] to elliptical orbits using the potential well, a concept originally introduced by Prussing and Coverstone [13].

The aim of this paper is to introduce a graphical approach for the preliminary deep space mission analysis of an electric sail (E-sail) [7,14,15], whose attitude is oriented in such a way to provide a purely radial thrust along the whole heliocentric trajectory. The space vehicle is therefore subjected to a propulsive outward acceleration that, according to the most recent studies [16], varies inversely proportional to the Sun–spacecraft distance r. Following Prussing and Coverstone [13], when the propulsion system is switched on, the spacecraft trajectory can be mapped into an "energy plane", that is, the plane in which the specific mechanical energy of the osculating orbit is expressed as a function of the spacecraft radial distance from the primary. In particular, Prussing and Coverstone [13] suggest to partition the energy plane into

* Corresponding author. Tel.: +39 050 2217258; fax: +39 050 2217244.
E-mail addresses: g.mengali@ing.unipi.it (G. Mengali), a.quarta@ing.unipi.it (A.A. Quarta), g.aliasi@dia.unipi.it (G. Aliasi).

0094-5765/$ - see front matter © 2012 Elsevier Ltd. All rights reserved.
http://dx.doi.org/10.1016/j.actaastro.2012.03.022

Please cite this article as: G. Mengali, et al., A graphical approach to electric sail mission design with radial thrust, Acta Astronautica (2012), http://dx.doi.org/10.1016/j.actaastro.2012.03.022

Nomenclature

a	semimajor axis
$a_\oplus$	E-sail characteristic acceleration
$\mathcal{E}$	specific mechanical energy of the osculating orbit
$\mathcal{E}_w$	potential well boundary
e	eccentricity
P	point in the energy plane
p	semilatus rectum
q	resonance ratio
R	prescribed distance
r	Sun–spacecraft distance ($r_\oplus \triangleq 1$ AU)
T	orbital period
t	time
u	radial component of velocity
V_∞	hyperbolic excess velocity
v	circumferential component of velocity
β	dimensionless characteristic acceleration
θ	polar angle
$\mu_\odot$	Sun's gravitational parameter
ω	argument of periapsis

Subscripts

0	initial, parking orbit
a	aphelion
b	point on the potential well boundary
e	escape
j	jettison
k	Keplerian
min	minimum
n	Near Earth Asteroid
p	perihelion
t	tangent
☊	ascending node
☋	descending node

Superscripts

$\dot{}$	time derivative
$\tilde{}$	dimensionless value
$\star$	critical value

allowed and forbidden regions using the so-called potential well, which bounds the radial distance interval within which the spacecraft motion is feasible.

With the aid of a suitable choice of the independent variables, another definition of the energy plane, slightly different than that of Ref. [13], is now introduced. In this new energy plane, the specific mechanical energy of an E-sail depends linearly on the distance from the Sun, and its slope is proportional to the E-sail characteristic acceleration, that is, the maximum propulsive acceleration at a Sun–spacecraft distance equal to 1 Astronomical Unit (AU). The main results of a preliminary mission analysis are thus obtained by simply intersecting the potential well boundary with the line corresponding to the specific mechanical energy level.

2. E-sail motion with radial thrust

Consider a spacecraft, of constant mass, that initially tracks a heliocentric closed parking orbit of semilatus rectum p_0 and eccentricity e_0. The spacecraft primary propulsion system is constituted by an E-sail with characteristic acceleration $a_\oplus$, which, by assumption, provides a radial outward thrust whose modulus is inversely proportional [16] to the Sun–spacecraft distance r.

The E-sail thrust is switched-on at $t = t_0 \triangleq 0$, and the succeeding spacecraft motion takes place in the plane of the parking orbit. The corresponding spacecraft equations of motion in a polar, heliocentric reference frame are [11,16]

$$\dot{r} = u \tag{1}$$

$$\dot{\theta} = \frac{\sqrt{\mu_\odot p_0}}{r^2} \tag{2}$$

$$\dot{u} = \frac{\mu_\odot}{r^2}\left(\frac{p_0}{r} - 1\right) + a_\oplus \frac{r_\oplus}{r} \tag{3}$$

where θ is the polar angle measured counterclockwise from the direction of the parking orbit's eccentricity vector, u is the radial component of the spacecraft velocity, $\mu_\odot$ is the Sun's gravitational parameter, and $r_\oplus \triangleq 1$ AU is a reference distance. In the special case of circular parking orbit ($e_0 = 0$), the polar angle θ is measured counterclockwise from the Sun–spacecraft direction at time t_0.

When Eq. (1) is substituted into (3), the following second order, nonlinear differential equation in the variable r is obtained:

$$\ddot{r} = \frac{\mu_\odot}{r^2}\left(\frac{p_0}{r} + \beta \frac{r}{r_\oplus} - 1\right) \tag{4}$$

where the dimensionless characteristic acceleration β is defined as

$$\beta = \frac{a_\oplus}{\mu_\odot / r_\oplus^2} \tag{5}$$

Note that β plays the same role in the E-sail performance characterization as the lightness number [17] does for solar (or photonic) sails, when an ideal force model [18] is assumed.

The boundary conditions of Eq. (4) are given by the Sun–spacecraft distance and the spacecraft radial component of velocity at the initial time t_0, that is

$$r_0 = \frac{p_0}{1 + e_0 \cos\theta_0}, \quad u_0 = \sqrt{\frac{\mu_\odot}{p_0}} e_0 \sin\theta_0 \tag{6}$$

where $\theta_0 \triangleq \theta(t_0)$ is the starting polar angle.

Please cite this article as: G. Mengali, et al., A graphical approach to electric sail mission design with radial thrust, Acta Astronautica (2012), http://dx.doi.org/10.1016/j.actaastro.2012.03.022

Taking into account the initial conditions (6), the first integral of the autonomous differential Eq. (4) is

$$\frac{u^2-u_0^2}{2}+\frac{\mu_\odot p_0}{2}\left(\frac{1}{r^2}-\frac{1}{r_0^2}\right)-\mu_\odot\left(\frac{1}{r}-\frac{1}{r_0}\right)-\beta\frac{\mu_\odot}{r_\oplus}\log\left(\frac{r}{r_0}\right)=0 \tag{7}$$

Introduce now the specific mechanical energy $\mathcal{E}$ of the spacecraft heliocentric osculating orbit

$$\mathcal{E}=\frac{u^2}{2}+\frac{\mu_\odot p_0}{2r^2}-\frac{\mu_\odot}{r} \tag{8}$$

and observe that Eq. (7) can be written in a compact form as

$$\mathcal{E}=\mathcal{E}_0+\beta\frac{\mu_\odot}{r_\oplus}\log\left(\frac{r}{r_0}\right) \tag{9}$$

where

$$\mathcal{E}_0\triangleq\mathcal{E}(t_0)=\frac{u_0^2}{2}+\frac{\mu_\odot p_0}{2r_0^2}-\frac{\mu_\odot}{r_0} \tag{10}$$

is the specific mechanical energy of the spacecraft parking orbit. Note that the last term in Eq. (9) coincides with the work, per unit of mass, of the E-sail propulsive thrust corresponding to the radial displacement $\Delta r=r-r_0$.

According to Prussing and Coverstone [13], Eq. (9) maps the spacecraft motion into the "energy plane", that is, the plane where the osculating orbit's specific mechanical energy $\mathcal{E}$ is expressed as a function of the radial distance r. In this plane the spacecraft motion is from below constrained by the so-called potential well [13], that is

$$\mathcal{E}\geq\mathcal{E}_w \tag{11}$$

where $\mathcal{E}_w$ is the minimum allowable value of the specific mechanical energy (corresponding to a given radial distance r) that is obtained from Eq. (8) by enforcing the condition [19] $u^2\geq 0$, viz.

$$\mathcal{E}_w=\frac{\mu_\odot p_0}{2r^2}-\frac{\mu_\odot}{r} \tag{12}$$

The spacecraft heliocentric motion is better described using a modified energy plane $(\tilde{\mathcal{E}},\tilde{r})$, which results from the introduction of the following dimensionless terms:

$$\tilde{\mathcal{E}}\triangleq\frac{\mathcal{E}}{\mu_\odot/r_0},\quad \tilde{\mathcal{E}}_w\triangleq\frac{\mathcal{E}_w}{\mu_\odot/r_0},\quad \tilde{r}\triangleq\log\left(\frac{r}{r_0}\right) \tag{13}$$

Bearing in mind Eq. (6), the expressions for $\tilde{\mathcal{E}}$ and $\tilde{\mathcal{E}}_w$ are

$$\tilde{\mathcal{E}}=\frac{e_0^2-1}{2(1+e_0\cos\theta_0)}+\beta\frac{p_0}{r_\oplus(1+e_0\cos\theta_0)}\tilde{r} \tag{14}$$

$$\tilde{\mathcal{E}}_w=\frac{(1+e_0\cos\theta_0)}{2}\exp(-2\tilde{r})-\exp(-\tilde{r}) \tag{15}$$

and Eq. (11) becomes

$$\tilde{\mathcal{E}}\geq\tilde{\mathcal{E}}_w \tag{16}$$

From Eq. (15) it is clear that the shape of the potential well boundary $\tilde{\mathcal{E}}_w=\tilde{\mathcal{E}}_w(\tilde{r})$ depends both on the parking orbit characteristics (through e_0) and on the initial spacecraft position θ_0, but it is independent of the E-sail performance (quantified through the parameter β). On the contrary, for a circular parking orbit ($e_0=0$) the function $\tilde{\mathcal{E}}_w$ is independent of θ_0.

Moreover, Eq. (14) states that the dimensionless specific mechanical energy is a linear function of $\tilde{r}$, and its slope is proportional to the dimensionless characteristic acceleration β. For a circular parking orbit ($\tilde{r}=0$), the initial value of the dimensionless specific mechanical energy is simply $\tilde{\mathcal{E}}=-1/2$.

A graphical interpretation of Eqs. (14) and (15) provides valuable insights into the spacecraft heliocentric trajectory without the need of integrating the equations of motion (1)–(3). This matter is now illustrated in detail with the aid of a number of mission applications.

3. Minimum propulsive acceleration to escape

As a first application of the previous concepts to an E-sail mission analysis, consider the problem of finding the minimum propulsive acceleration required to escape from the Sun when the propulsion system is operating for the whole mission duration. This is a classical problem that has been extensively studied in the literature, especially under the assumption of constant propulsive, outward, acceleration [11,13,19]. Here the minimum value of $a_\oplus$ [equivalently, the minimum β, see Eq. (5)] will be found graphically in the energy plane. The two cases of circular or elliptic parking orbit will be discussed separately.

3.1. Circular parking orbit

The shape of the potential well $\tilde{\mathcal{E}}_w=\tilde{\mathcal{E}}_w(\tilde{r})$ for a circular parking orbit of radius $r_0\equiv p_0$ is shown in Fig. 1. Recall that the points below the potential well boundary belong to a forbidden region (shaded area in Fig. 1) where the spacecraft motion cannot take place.

According to Eq. (14), at the initial time t_0 the spacecraft position in the energy plane is represented by the point $P_0=(0,-1/2)$, and the spacecraft radial velocity component at t_0 is zero. When the propulsion system is switched-on ($t>t_0$), the spacecraft at first increases both its specific energy $\tilde{\mathcal{E}}$ and its distance from the Sun $\tilde{r}$ moving along the straight line defined by Eq. (14). This line will be

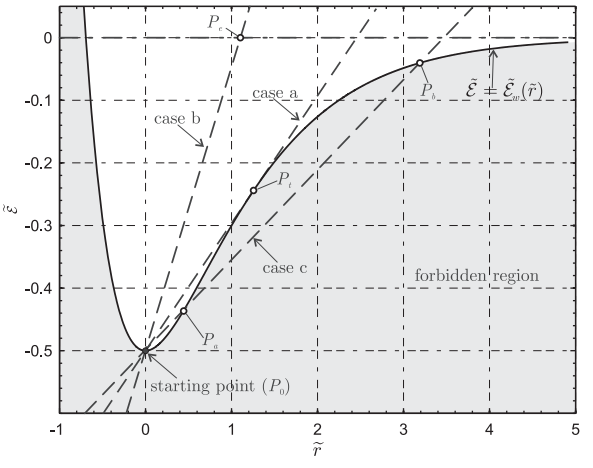

Fig. 1. Potential well boundary for a circular parking orbit.

Please cite this article as: G. Mengali, et al., A graphical approach to electric sail mission design with radial thrust, Acta Astronautica (2012), http://dx.doi.org/10.1016/j.actaastro.2012.03.022

referred to as "energy line", and its slope is proportional to the dimensionless characteristic acceleration β. The spacecraft motion corresponds to one of the following three cases.

3.1.1. Case a

The energy line, with a slope $\beta^\star r_0/r_\oplus$, is tangent to the potential well boundary at point $P_t=(\tilde{r}_t,\tilde{\mathcal{E}}_t)$, see Fig. 1. In this case, the pair $(\tilde{r}_t,\beta^\star)$ is solution of the system of algebraic equations

$$\tilde{\mathcal{E}}=\tilde{\mathcal{E}}_w \cap \frac{\partial\tilde{\mathcal{E}}}{\partial\tilde{r}}=\frac{\partial\tilde{\mathcal{E}}_w}{\partial\tilde{r}} \tag{17}$$

or, with the aid of Eqs. (14) and (15)

$$2\tilde{r}_t\exp(-\tilde{r}_t)[1-\exp(-\tilde{r}_t)-1=\exp(-\tilde{r}_t)[\exp(-\tilde{r}_t)-2] \tag{18}$$

$$\beta^\star=\left(\frac{r_\oplus}{r_0}\right)\exp(-\tilde{r}_t)[1-\exp(-\tilde{r}_t)] \tag{19}$$

whose solution is

$$\tilde{r}_t\simeq 1.256431,\quad \beta^\star\simeq 0.203632\left(\frac{r_\oplus}{r_0}\right) \tag{20}$$

Substituting $\tilde{r}_t$ from (20) into Eq. (14), the energy at P_t is $\tilde{\mathcal{E}}_t\simeq -0.244150$.

The spacecraft motion can now be qualitatively described as follows. When the propulsion system (whose dimensionless characteristic acceleration is $\beta^\star$, see Eq. (20)) is switched-on, the Sun–spacecraft distance increases following the segment $\overline{P_0P_t}$. At time t_t the spacecraft reaches the point P_t whose distance from the Sun is

$$r_t\triangleq r_0\exp(\tilde{r}_t)\simeq 3.512862r_0 \tag{21}$$

here the spacecraft radial velocity component is zero, because P_t belongs to the potential well boundary, while its radial acceleration component $\ddot{r}_t\triangleq\ddot{r}(r_t)$ is obtained from Eq. (4) with the substitution $\beta=\beta^\star$ and $r=r_t$. It can be verified that $\ddot{r}_t=0$. Therefore, the spacecraft reaches P_t with zero velocity and zero acceleration in the radial direction. Accordingly, for $t\geq t_t$ the spacecraft tracks a circular, non-Keplerian [6,20], orbit of radius r_t with a constant velocity $v=\sqrt{\mu_\odot p_0}/r_t$, as is shown in Fig. 2.

From Eq. (21), the orbital period T_t of the non-Keplerian orbit is

$$T_t=\frac{2\pi}{\sqrt{\mu_\odot/r_0^3}}\exp(2\tilde{r}_t) \tag{22}$$

A linear stability analysis reveals that this non-Keplerian orbit is unstable. In fact, from Eq. (4), the derivative of the radial acceleration component is

$$\frac{\partial\ddot{r}}{\partial r}=\frac{\mu_\odot}{r_0^2}[2\exp(-2\tilde{r})-3\exp(-3\tilde{r})-\beta(r_0/r_\oplus)\exp(-\tilde{r})] \tag{23}$$

Therefore, when $\beta=\beta^\star$ and $\tilde{r}=\tilde{r}_t$, Eq. (23) states that $\partial\ddot{r}/\partial r\simeq 0.0349\mu_\odot/r_0^2>0$.

To summarize, in this case the spacecraft heliocentric trajectory presents a single perihelion point (P_0 in the energy plane) at a distance r_0 from the Sun, and the maximum attainable distance (r_t) depends linearly on r_0.

3.1.2. Case b

When the slope of the energy line is sufficiently high (that is, $\beta>\beta^\star$), P_0 is the only intersection point between the energy line and the potential well boundary, see Fig. 1. In this case, for all $t>t_0$, the spacecraft is pushed away from the Sun and eventually reaches the escape condition $\tilde{\mathcal{E}}=0$ at a distance [see Eqs. (13) and (14)]

$$r_e=r_0\exp\left(\frac{r_\oplus}{2\beta r_0}\right) \tag{24}$$

If the mission requirement is to reach a given hyperbolic excess velocity V_∞ with respect to the Sun, the E-sail can be jettisoned when the Sun–spacecraft distance is

$$r=r_0\exp\left(\frac{r_\oplus V_\infty^2+\mu_\odot r_\oplus/r_0}{2\mu_\odot\beta}\right) \tag{25}$$

In this case, P_0 is the only trajectory point in which the radial velocity component is zero and r_0 is the corresponding perihelion distance. Fig. 3 shows the spacecraft heliocentric trajectory when $\beta=1.1\beta^\star\simeq 0.223995r_\oplus/r_0$. Note that, according to Eq. (24), the escape condition occurs at a distance $r_e\simeq 9.3r_0$ from the Sun.

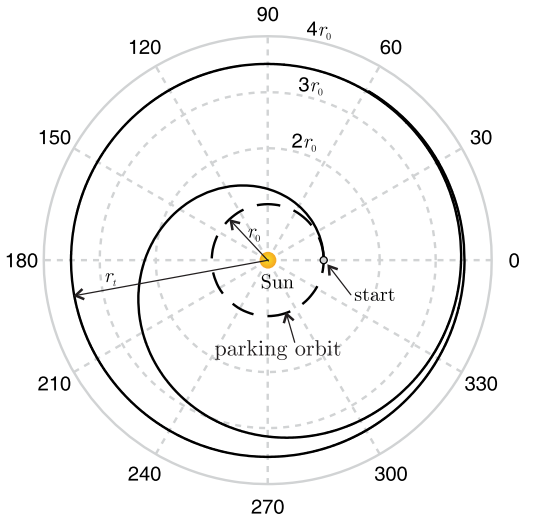

Fig. 2. Spacecraft trajectory for $\beta=\beta^\star$, starting from a circular parking orbit of radius r_0.

3.1.3. Case c

The last case is obtained when the energy line intercepts the potential well boundary at three points, P_0, $P_a=(\tilde{r}_a,\tilde{\mathcal{E}}_a)$ and $P_b=(\tilde{r}_b,\tilde{\mathcal{E}}_b)$, as is shown in Fig. 1. This situation is representative of a low-performance propulsion system, that is, an E-sail with a low characteristic acceleration ($\beta<\beta^\star$). The values of $\tilde{r}_a$ and $\tilde{r}_b$, with $0<r_a<r_t<r_b$, are two of the three real solutions of the nonlinear equation $\tilde{\mathcal{E}}=\tilde{\mathcal{E}}_w$, where $\tilde{\mathcal{E}}$ is given by Eq. (14) and $\tilde{\mathcal{E}}_w$ by Eq. (15). The nonlinear equation $\tilde{\mathcal{E}}=\tilde{\mathcal{E}}_w$ in the unknown $\tilde{r}$ can be solved numerically, and the solution $\tilde{r}=0$ can be discarded as it coincides with r_0. The least of the remaining two solutions corresponds to $\tilde{r}_a$, that is, the aphelion distance. To simplify the succeeding spacecraft trajectory analysis, Fig. 4 shows the values of aphelion distance r_a/r_0 as a function of the dimensionless characteristic acceleration $\beta<\beta^\star$. The same figure also shows

Please cite this article as: G. Mengali, et al., A graphical approach to electric sail mission design with radial thrust, Acta Astronautica (2012), http://dx.doi.org/10.1016/j.actaastro.2012.03.022

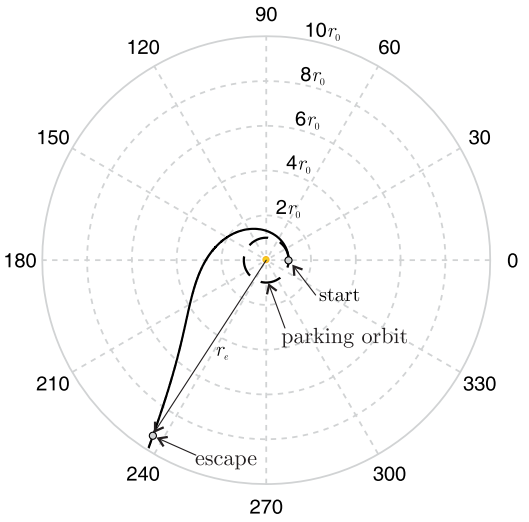

Fig. 3. Spacecraft trajectory for $\beta = 1.1\beta^\star \simeq 0.223995 r_\oplus / r_0$, starting from a circular parking orbit of radius r_0.

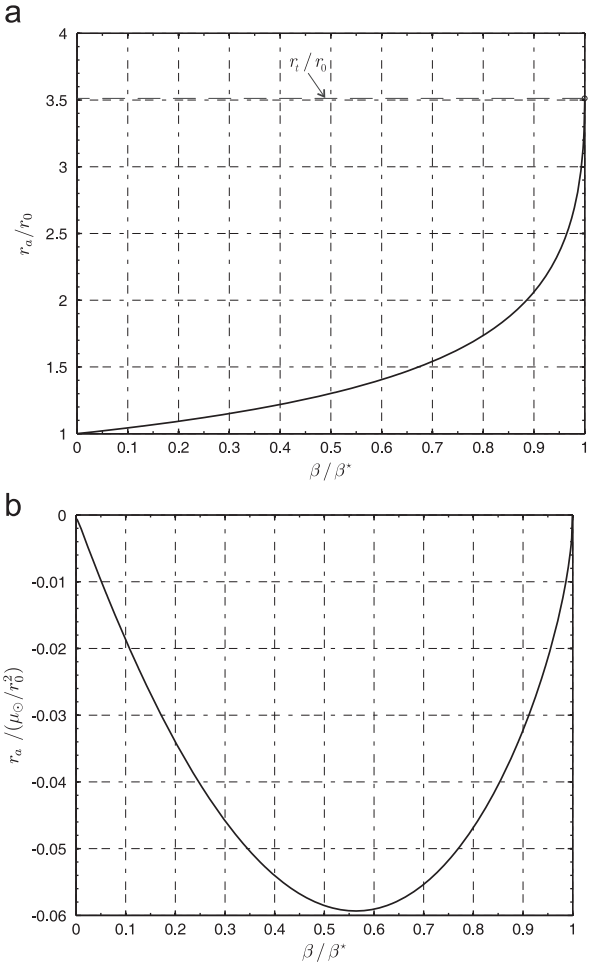

Fig. 4. Aphelion distance and radial component of acceleration as a function of the dimensionless characteristic acceleration for a circular parking orbit of radius r_0. (a) Aphelion distance, (b) radial component of acceleration.

the spacecraft radial acceleration component, which can be obtained from Eq. (4) when $r = r_a$.

Fig. 4(b) shows that $\ddot{r}_a < 0$ for $\beta \in (0, \beta^\star)$, whereas $\ddot{r}_a = 0$ when $\beta = \{0, \beta^\star\}$. The special case of $\beta = 0$ is of scarce importance, as it corresponds to a spacecraft without any propulsion system. In that case the spacecraft tracks the initial circular parking orbit and the energy line reduces to the point P_0.

The spacecraft motion can be described as follows. Assuming that $\beta \in (0, \beta^\star)$, for $t > t_0$ the spacecraft increases its distance from the Sun until, at time t_a, it reaches a distance $r_a < r_t$ (point P_a of Fig. 1). During this phase the spacecraft tracks, in the energy plane, the segment $\overline{P_0 P_a}$. Because P_a belongs to the potential well boundary, at P_a the spacecraft radial velocity component is zero, but the radial acceleration component is negative (see Fig. 4(b)). Therefore the spacecraft is subjected to a net inward force, proportional to $\ddot{r}_a$, that curves the trajectory towards the Sun. As a result the distance from the Sun starts decreasing and the spacecraft tracks backwards the segment $\overline{P_0 P_a}$ until it reaches P_0 again (at time t_1). Note that the spacecraft polar angle $\theta_1 \triangleq \theta(t_1)$ is, in general, different from $\theta_0 + 2k\pi$, where k is a positive integer. For $t > t_1$ the motion in the energy plane repeats, that is, the spacecraft increases its distance from the Sun until r_a and so on. In other words the spacecraft oscillates indefinitely, in the energy plane, along the segment $\overline{P_0 P_a}$. Clearly, the point P_b cannot be reached because the segment $\overline{P_a P_b}$ lies in the forbidden region. Therefore, the value of $\beta^\star$, given by Eq. (20), is the minimum dimensionless characteristic acceleration required to escape from the circular parking orbit of radius r_0. In addition, r_t is the maximum aphelion distance of a closed orbit when the propulsion system is on. When viewed with respect to a heliocentric reference frame, the spacecraft trajectory is constrained within the region between the two circles of radius r_0 (perihelion) and r_a (aphelion). For example Fig. 5 illustrates the spacecraft trajectory for $\beta = 0.9\beta^\star \simeq 0.183269 r_\oplus / r_0$, in which the aphelion distance is $r_a \simeq 2.06 r_0$, a value which is in agreement with Fig. 4(a).

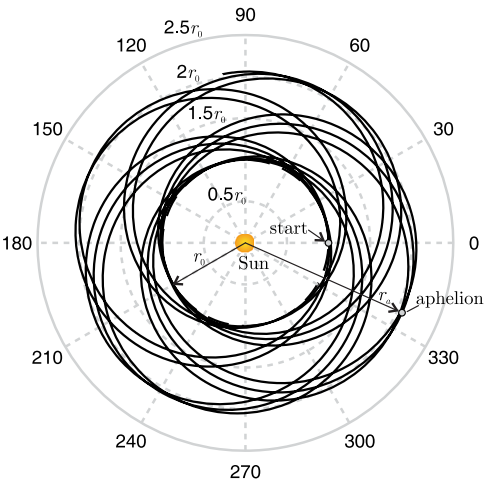

Fig. 5. Spacecraft trajectory for $\beta = 0.9\beta^\star \simeq 0.183268 r_\oplus / r_0$, starting from a circular parking orbit of radius r_0.

Please cite this article as: G. Mengali, et al., A graphical approach to electric sail mission design with radial thrust, Acta Astronautica (2012), http://dx.doi.org/10.1016/j.actaastro.2012.03.022

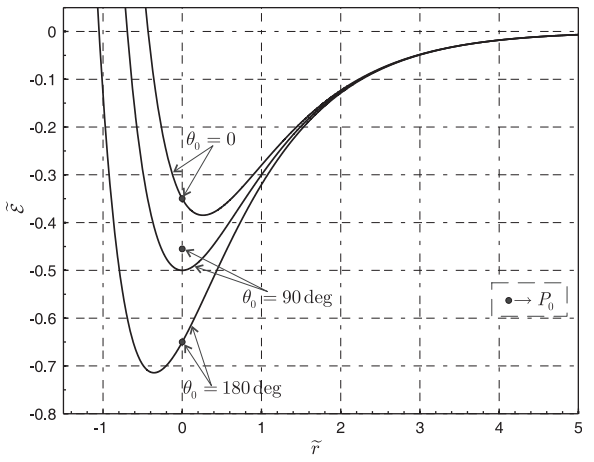

Fig. 6. Potential well boundary and starting point P_0, for three values of the polar angle θ_0, starting from an elliptic orbit of eccentricity $e_0=0.3$.

3.2. Elliptic parking orbit

If the parking orbit is elliptic, that is, $e_0 \in [0, 1)$, both the potential well boundary and the energy line location depend on the starting polar angle θ_0, see Eqs. (14) and (15). For a given value of e_0 the position of P_0 in the energy plane changes with θ_0 as is shown in Fig. 6 for $e_0=0.3$. Note that when $\theta_0 \in \{0, 180\}^\circ$ the point P_0 belongs to the potential well boundary, whereas for $\theta_0 \in (0, 180)^\circ$ the point P_0 is inside the allowable region.

For a given quadruple (p_0,e_0,θ_0,β) the potential well boundary and the energy line are univocally defined, and the analysis of the spacecraft motion coincides with that described in the last section. In particular, the minimum value $\beta^\star$ of the dimensionless characteristic acceleration required to escape from the Sun is now a function of the triplet (p_0,e_0,θ_0). Bearing in mind Eqs. (14) and (15), the numerical solutions of Eq. (17) have been summarized in Fig. 7 where, for symmetry reasons, the analysis of the initial polar angle range has been confined to $\theta_0 \in [0, 180]^\circ$.

A few remarks are in order. For a circular parking orbit, both $\beta^\star$ and $\tilde{r}_t$ are constant with respect to the starting polar angle θ_0, and their values are in agreement with Eq. (20). More important, Fig. 7(a) shows that, for a given value of the pair (p_0,e_0), the parameter $\beta^\star$ increases with θ_0. Therefore, for a given parking orbit, the minimum value of the dimensionless characteristic acceleration $\beta^\star_{\min} \triangleq \min[\beta^\star(\theta_0)]$ is obtained when $\theta_0 = 0$, that is, when the propulsion system is switched-on at the initial perihelion [12]. Fig. 8 shows the required value of $\beta^\star_{\min}$ as a function of p_0 and e_0.

The quantity $\beta^\star_{\min} p_0/r_\oplus$ is almost linear with e_0, and can be approximated (with errors less than 0.6%) by the function

$$\beta^\star_{\min} \frac{p_0}{r_\oplus} \simeq -0.2036 e_0 + 0.2036 \tag{26}$$

Fig. 8 and Eq. (26) reveal that $\beta^\star_{\min} \to 0$ as $e_0 \to 1$. However this corresponds to the special case of a parabolic parking orbit and, indeed, the spacecraft reaches the escape

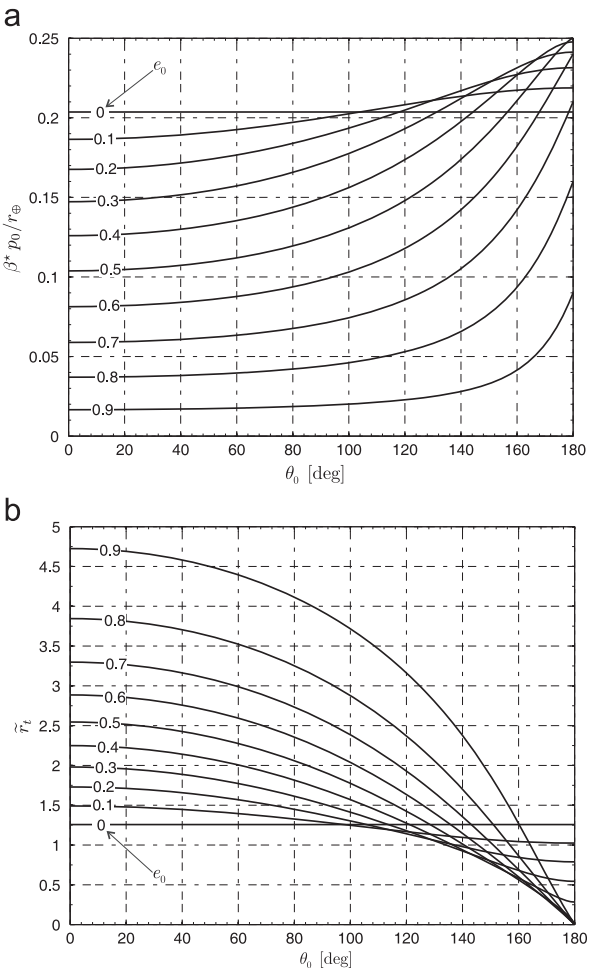

Fig. 7. Optimal performance for an escape mission as a function of the parking orbit characteristics (p_0,e_0) and the initial polar angle θ_0. (a) Dimensionless characteristic acceleration $\beta^\star$, (b) non-Keplerian orbit dimensionless radius $\tilde{r}_t$.

condition at $t=0$ without the need of any propulsion system.

As an example, if the elliptic parking orbit coincides with Earth's heliocentric orbit of semimajor axis $a_0 = 1$ AU and eccentricity $e_0 = 0.0167102$, one obtains that $\beta^\star_{\min} \simeq 0.201$ (the characteristic acceleration is $1.19\,\text{mm/s}^2$). Starting instead from Mercury's heliocentric orbit ($a_0 = 0.3870989$ AU and $e_0 = 0.2056307$) the value of $\beta^\star_{\min}$ increases to about 0.449 and the minimum characteristic acceleration required to escape is $2.662\,\text{mm/s}^2$.

4. Attainment of a given distance from the Sun

As a second practical application of the potential well's concept consider now the problem of finding the minimum characteristic acceleration required to reach a prescribed distance R from the Sun. Without any loss of generality, a circular parking orbit of radius r_0 is assumed. Indeed, the extension to an elliptic parking orbit is straightforward. Unlike the previous analysis, in this case the propulsion system can be switched-off one time along

Please cite this article as: G. Mengali, et al., A graphical approach to electric sail mission design with radial thrust, Acta Astronautica (2012), http://dx.doi.org/10.1016/j.actaastro.2012.03.022

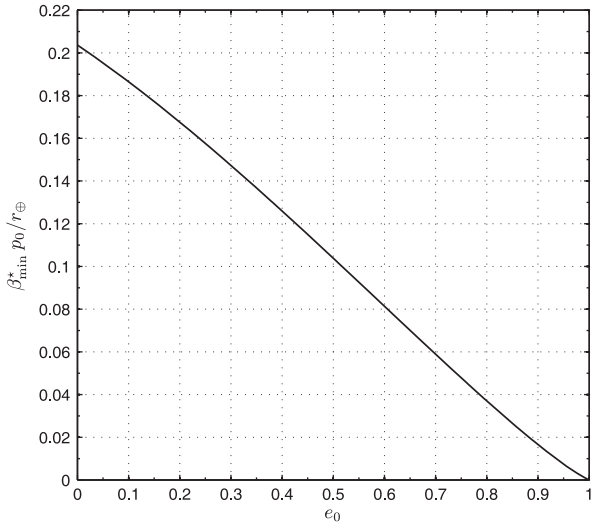

Fig. 8. Minimum dimensionless characteristic acceleration $\beta^*_{\min}$ required to escape from the Sun, as a function of the parking orbit characteristics p_0 and e_0.

the trajectory to model a situation in which the E-sail is jettisoned. To solve the problem, it is useful to distinguish between the following three cases.

4.1. Case a

Assume first that $\tilde{R} \in (0,\tilde{r}_t]$, where $\tilde{r}_t$ is given by Eq. (20). In the energy plane the parking orbit is defined by the point $P_0 = (0,-1/2)$ while the target point belongs to a vertical line of equation $\tilde{r} = \tilde{R}$. The dimensionless specific mechanical energy at the intersection point $P_R = (\tilde{R},\tilde{\mathcal{E}}_R)$ between this vertical line and the potential well boundary is obtained from Eq. (15)

$$\tilde{\mathcal{E}}_R = \tfrac{1}{2}\exp(-2\tilde{R}) - \exp(-\tilde{R}) \tag{27}$$

with $\tilde{\mathcal{E}}_R > -1/2$ for $\tilde{R} > 0$. Because for $t > t_0$ the spacecraft tracks an energy line whose slope is proportional to the dimensionless characteristic acceleration [see Eq. (14)], the value of $\beta_{\min}$ is

$$\beta_{\min} = \frac{r_\oplus}{\tilde{R} r_0}(\tilde{\mathcal{E}}_R + 1/2) \equiv \frac{r_\oplus}{2\tilde{R} r_0}[\exp(-2\tilde{R}) - 2\exp(-\tilde{R}) + 1] \tag{28}$$

In other terms, when $\beta = \beta_{\min}$ the spacecraft moves along the segment $\overline{P_0 P_R}$, and reaches the target distance $\tilde{R}$ at the aphelion of the transfer trajectory, as is shown in Fig. 9.

For example, assume that $R = 1.524$ AU (a value corresponding to the Sun–Mars mean distance), and a parking circular orbit of radius $r_0 \equiv r_\oplus$. In this case $\tilde{R} \simeq 0.421338$ and, from Eq. (28), $\beta_{\min} \simeq 0.140291$, that is, $a_\oplus \simeq 0.832$ mm/s^2. The spacecraft transfer trajectory is shown in Fig. 10.

4.2. Case b

If $\tilde{R} > \tilde{r}_t$, a portion of the segment $\overline{P_0 P_R}$ belongs to the forbidden region of the energy plane and the previous transfer strategy fails. In this case, as P_R is on the right of P_t (see Fig. 11), the optimal solution is simply the energy

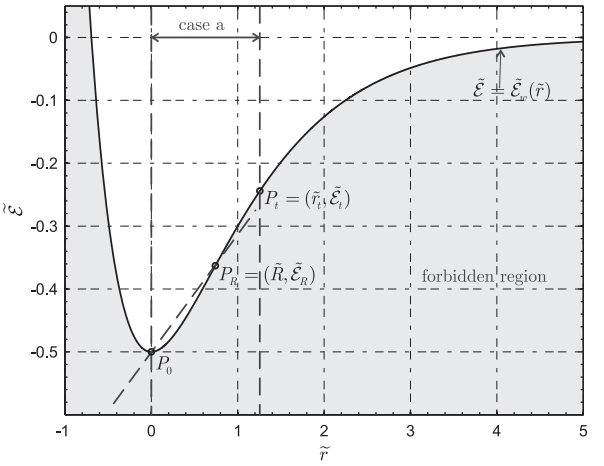

Fig. 9. Optimal strategy to reach a (dimensionless) distance $\tilde{R} \in (0,\tilde{r}_t]$, starting from a circular parking orbit.

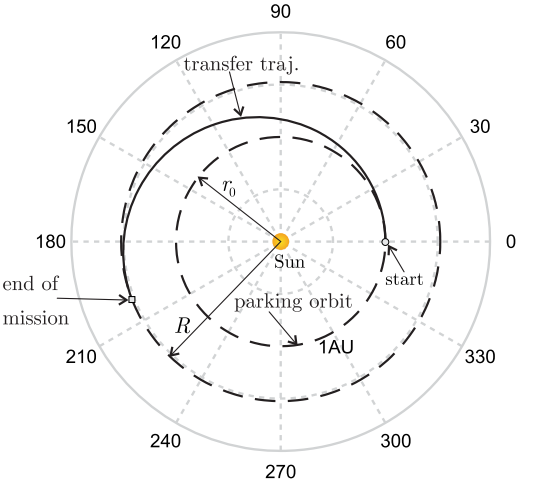

Fig. 10. Optimal transfer trajectory to reach a distance $R = 1.524$ AU, starting from a circular parking orbit of radius $r_0 = r_\oplus$.

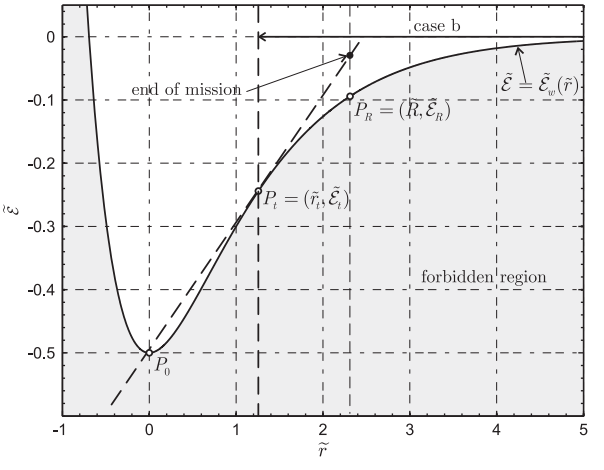

Fig. 11. Optimal strategy to reach a (dimensionless) distance $\tilde{R} > \tilde{r}_t$, starting from a circular parking orbit.

Please cite this article as: G. Mengali, et al., A graphical approach to electric sail mission design with radial thrust, Acta Astronautica (2012), http://dx.doi.org/10.1016/j.actaastro.2012.03.022

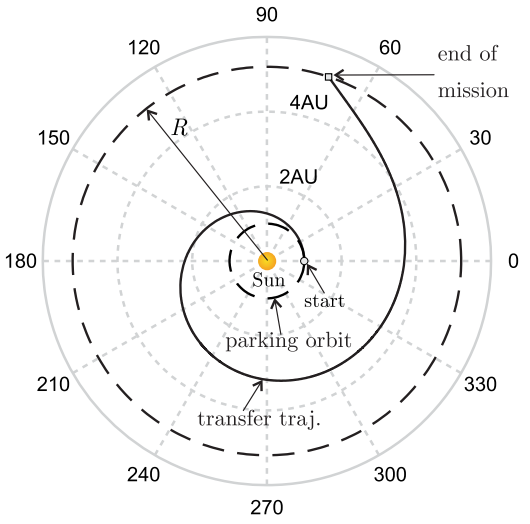

Fig. 12. Optimal transfer trajectory to reach a distance $R = 5.2$ AU, starting from a circular parking orbit of radius $r_0 = r_\oplus$.

line that passes through P_0 and P_t. From Eq. (20), the minimum value of the dimensionless characteristic acceleration is

$$\beta_{\min} > 0.203632\left(\frac{r_\oplus}{r_0}\right) \tag{29}$$

Assuming $R = 5.2$ AU, equal to the Sun–Jupiter mean distance, and $r_0 \equiv r_\oplus$, the dimensionless distance is $\tilde{R} \simeq 1.648658$ and the minimum characteristic acceleration is $a_\oplus \simeq 1.2087$ mm/s^2. The spacecraft transfer trajectory is shown in Fig. 12.

4.3. Case c

Finally, assume that the target distance is less than r_0, or $\tilde{R} < 0$. In this case a transfer without an E-sail jettison is unfeasible, because the propulsion system provides an outward radial thrust only. However the target distance can be reached using a Keplerian orbit whose perihelion distance is $r_p \le R$. Because the spacecraft can be transferred only towards Keplerian orbits whose semilatus rectum is $p_0 \equiv r_0$, the equation $r_p \le R$ represents a constraint on the minimum aphelion radius r_a of the candidate Keplerian orbit, that is

$$r_a \ge \frac{r_0 R}{2R - r_0} \tag{30}$$

In particular, Eq. (30) states that the spacecraft cannot reach a distance from the Sun less than $r_0/2$.

Assuming $R > r_0/2$ (that is, $\tilde{R} > \log(1/2) \simeq -0.6931$), from a geometric viewpoint the optimal mission strategy corresponds to transfer the spacecraft to a Keplerian orbit whose perihelion radius r_p is equal to R. For a given value of $r_p = R$, the corresponding Keplerian orbit is represented, in the energy plane, by a horizontal segment ranging from $P_p = (\tilde{R}, \tilde{\mathcal{E}}_R)$ to $P_a = (\tilde{r}_a, \tilde{\mathcal{E}}_R)$, see Fig. 13, where

$$\tilde{r}_a \triangleq \log\left(\frac{R}{2R - r_0}\right) \tag{31}$$

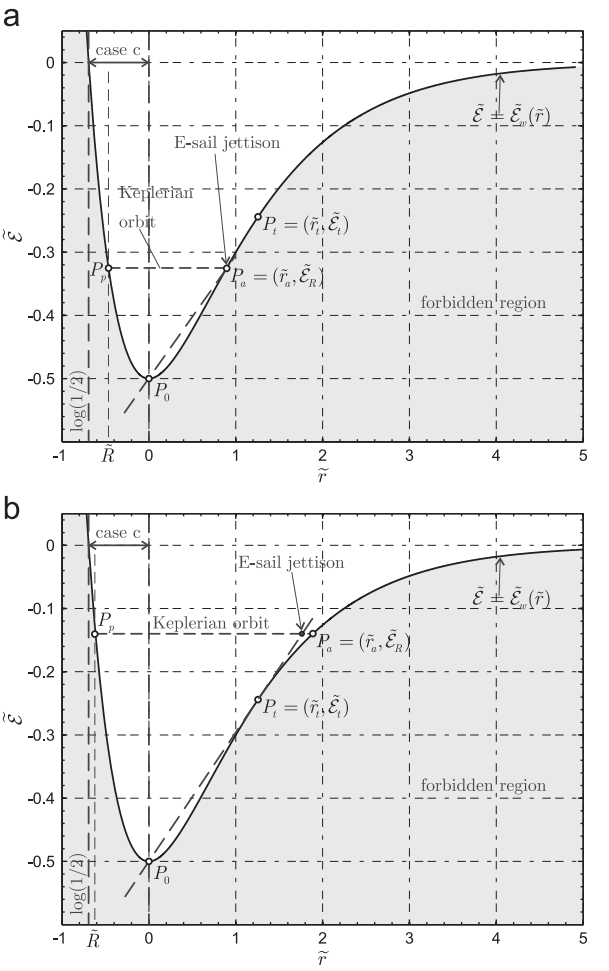

Fig. 13. Optimal strategy to reach a (dimensionless) distance $\tilde{R} \in (\log(1/2), 0)$ as a function of $\tilde{r}_a$, starting from a circular parking orbit. (a) $\tilde{r}_a < \tilde{r}_t$, (b) $\tilde{r}_a > \tilde{r}_t$.

and $\tilde{\mathcal{E}}_R$ is given by Eq. (27). Note that P_p and P_a map, in the energy plane, the perihelion and the aphelion point of the Keplerian orbit, respectively.

The minimum value of the dimensionless characteristic acceleration required to reach a point of the segment $\overline{P_p P_a}$ depends on the horizontal position of P_a, that is, on the value of $\tilde{r}_a$. In fact, for $\tilde{r}_a \le \tilde{r}_t$, with $\tilde{r}_t$ given by Eq. (21), the minimum value of β corresponds to the transfer orbit that reaches the Keplerian orbit at its aphelion P_a, viz.

$$\beta_{\min} = \frac{r_\oplus}{\tilde{r}_a r_0}(\tilde{\mathcal{E}}_R + 1/2) \equiv \frac{r_\oplus}{2\tilde{r}_a r_0}[\exp(-2\tilde{R}) - 2\exp(-\tilde{R}) + 1] \tag{32}$$

The E-sail is jettisoned exactly at a distance r_a from the Sun, where r_a is given by the right hand side of Eq. (30). This strategy is summarized in Fig. 13(a). For example, if $R = 0.723$ AU, equal to the Sun–Venus mean distance, and $r_0 \equiv r_\oplus$, the target distance is $\tilde{R} \simeq -0.324346$ and $\tilde{r}_a \simeq 0.483090 < \tilde{r}_t$. From Eq. (32), the minimum dimensionless characteristic acceleration is $\beta_{\min} \simeq 0.1519$ (that is $a_\oplus \simeq 0.901$ mm/s^2), and the spacecraft transfer trajectory is

Please cite this article as: G. Mengali, et al., A graphical approach to electric sail mission design with radial thrust, Acta Astronautica (2012), http://dx.doi.org/10.1016/j.actaastro.2012.03.022

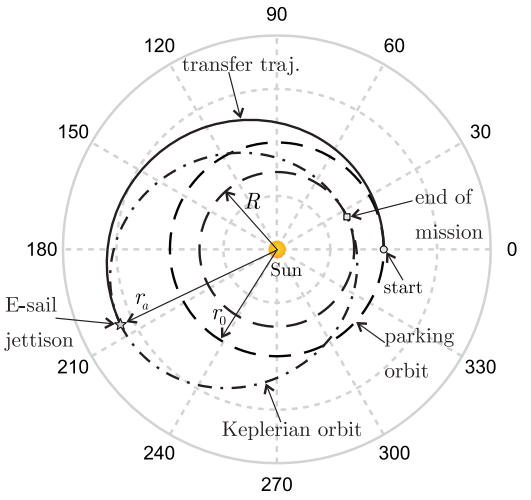

Fig. 14. Optimal transfer trajectory to reach a distance $R=0.723$ AU, starting from a circular parking orbit of radius $r_0=r_\oplus$.

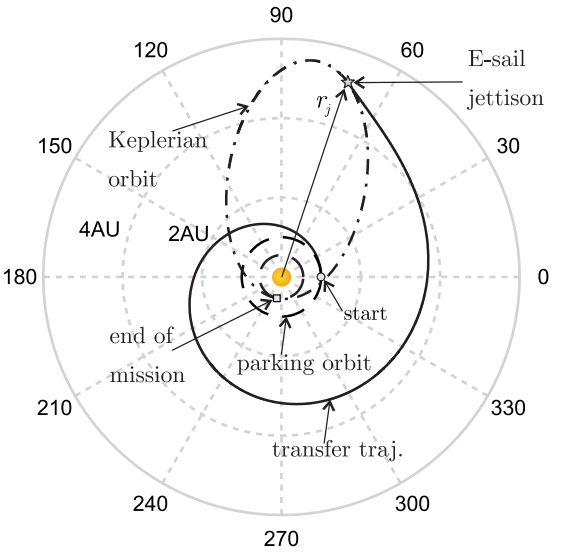

Fig. 15. Optimal transfer trajectory to reach a distance $R=0.55$ AU, starting from a circular parking orbit of radius $r_0=r_\oplus$.

shown in Fig. 14 along with the corresponding Keplerian orbit.

As was discussed in Case b, when $\tilde{r}_a > \tilde{r}_t$ the minimum dimensionless characteristic acceleration is equal to $\beta^\star$, see Eq. (29), and the E-sail is jettisoned at a distance $r_j < r_a$. This situation is illustrated in Fig. 13(b) and the jettison distance is

$$r_j = r_0 \exp\left(\frac{\tilde{\mathcal{E}}_R + 1/2}{\beta^\star r_0/r_\oplus}\right) \equiv r_0 \exp\left(\frac{\exp(-2\tilde{R}) - 2\exp(-\tilde{R}) + 1}{2\beta^\star r_0/r_\oplus}\right) \tag{33}$$

For example, if $r_0 \equiv r_\oplus$ and $R=0.55$ AU ($\tilde{R} \simeq -0.597837$), the E-sail jettison distance is $r_j \simeq 5.174$ AU and the transfer trajectory is shown in Fig. 15.

5. Reaching a Keplerian orbit of given period

The third practical application of the potential well's concept is the study of the minimum characteristic acceleration $\beta_{\min}$ required to reach a heliocentric Keplerian closed orbit of given period T_k. By assumption, the target Keplerian orbit is coplanar to the circular parking orbit of radius r_0. Moreover, the E-sail can be jettisoned at a suitable point of the transfer trajectory.

As discussed in the previous section, the target Keplerian orbit in the energy plane is represented by a horizontal segment whose dimensionless specific mechanical energy $\tilde{\mathcal{E}}_k$ is

$$\tilde{\mathcal{E}}_k \triangleq -\frac{r_0}{2\sqrt[3]{T_k^2\mu_\odot/(4\pi^2)}} \tag{34}$$

The segment endpoints, $P_p=(\tilde{r}_p,\tilde{\mathcal{E}}_k)$ and $P_a=(\tilde{r}_a,\tilde{\mathcal{E}}_k)$, map the target Keplerian orbit perihelion and aphelion points, respectively, where $\tilde{r}_p=\log(r_p/r_0)$ and $\tilde{r}_a=\log(r_a/r_0)$ with

$$r_p = \sqrt[3]{T_k^2\mu_\odot/(4\pi^2)}\left(1-\sqrt{1-\frac{r_0}{\sqrt[3]{T_k^2\mu_\odot/(4\pi^2)}}}\right) \tag{35}$$

$$r_a = \sqrt[3]{T_k^2\mu_\odot/(4\pi^2)}\left(1+\sqrt{1-\frac{r_0}{\sqrt[3]{T_k^2\mu_\odot/(4\pi^2)}}}\right) \tag{36}$$

In fact, because the semilatus rectum p_k of the target Keplerian orbit is equal to r_0, the semimajor axis a_k and the eccentricity e_k of the final orbit are obtained as

$$a_k = \sqrt[3]{T_k^2\mu_\odot/(4\pi^2)} \tag{37}$$

$$e_k = \sqrt{1-\frac{r_0}{a_k}} \equiv \sqrt{1-\frac{r_0}{\sqrt[3]{T_k^2\mu_\odot/(4\pi^2)}}} \tag{38}$$

Note that the constraint $p_k=r_0$ implies that a transfer towards an orbit of period $T_k < T_0 \triangleq 2\pi\sqrt{r_0^3/\mu_\odot}$ (or $\tilde{\mathcal{E}}_k < -1/2$) is infeasible. Therefore assume that $T_k > T_0$, as $T_k = T_0$ corresponds to a situation in which at time t_0 the spacecraft is already on the target Keplerian orbit. The problem can be solved in the energy plane with the aid of the two cases illustrated in Fig. 16.

5.1. Case a

The dimensionless specific mechanical energy of the target Keplerian orbit ranges in the interval $\tilde{\mathcal{E}}_k \in (-1/2, \tilde{\mathcal{E}}_t]$, where $\tilde{\mathcal{E}}_t \simeq -0.244150$ is the ordinate of point P_t. In this case $\tilde{r}_a \le \tilde{r}_t$ and, as was discussed in the previous section, the optimal strategy is to reach the Keplerian orbit aphelion where the E-sail is jettisoned. The minimum required dimensionless characteristic acceleration is

$$\beta_{\min} = \frac{r_\oplus}{\tilde{r}_a r_0}(\tilde{\mathcal{E}}_k + 1/2) \tag{39}$$

and the jettison distance is $r_j = r_a$, see Eq. (36).

Please cite this article as: G. Mengali, et al., A graphical approach to electric sail mission design with radial thrust, Acta Astronautica (2012), http://dx.doi.org/10.1016/j.actaastro.2012.03.022

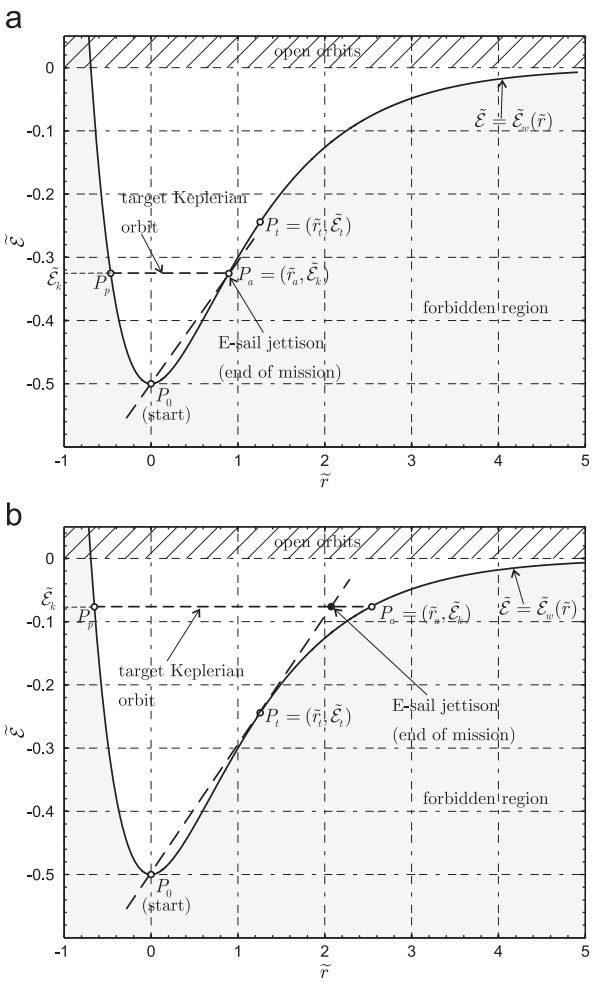

Fig. 16. Optimal strategy to reach a heliocentric (closed) Keplerian orbit of given period, starting from a circular parking orbit. (a) Case a and (b) Case b.

5.2. Case b

The dimensionless specific mechanical energy of the target Keplerian orbit ranges in the interval $\tilde{\mathcal{E}}_k \in (\tilde{\mathcal{E}}_t, 0)$, that is, the dimensionless aphelion radius is greater than $\tilde{r}_t$. In this case the optimal strategy requires that $\beta_{\min} = \beta^\star$ [see Eq. (20)], and the jettison distance r_j is given by

$$r_j = r_0 \exp\left(\frac{\tilde{\mathcal{E}}_k + 1/2}{\beta^\star r_0/r_\oplus}\right) \tag{40}$$

The previous relationships are useful for a preliminary mission analysis whose aim is to reach a Keplerian orbit in mean motion orbital resonance with the parking one. The transfer trajectory characteristics and the E-sail required performances have been summarized in Table 1 for some values of resonance ratio T_k/T_0. The resonance ratio corresponds to the number of spacecraft revolutions for one revolution of the given celestial body around the Sun. Note that for a given value of r_0, both the dimensionless characteristic acceleration $\beta_{\min}$ and the jettison distance r_j increase with the resonance ratio T_k/T_0. In fact, an increment of the period T_k increases both $\tilde{\mathcal{E}}_k$ and r_a.

Table 1
Optimal performance to obtain a mean motion orbital resonance with the parking orbit.

T_k/T_0	r_p/r_0	r_a/r_0	$\beta_{\min} r_0/r_\oplus$	r_j/r_0	Case
2	0.6218	2.5530	0.1974	2.5530	a
3	0.5812	3.5790	0.2036	3.5786	b
4	0.5629	4.4768	0.2036	4.3972	b
5	0.5521	5.2959	0.2036	5.0313	b
6	0.5450	6.0589	0.2036	5.5388	b
7	0.5398	6.7788	0.2036	5.9560	b
8	0.5359	7.4641	0.2036	6.3063	b
9	0.5328	8.1207	0.2036	6.6056	b
10	0.5303	8.7529	0.2036	6.8648	b
3:2	0.6726	1.9481	0.1776	1.9481	a
5:2	0.5966	3.0874	0.2027	3.0874	a
7:2	0.5706	4.0398	0.2036	4.0159	b
9:2	0.5569	4.8945	0.2036	4.7330	b
4:3	0.7053	1.7175	0.1613	1.7175	a
5:3	0.6505	2.1609	0.1873	2.1609	a
7:3	0.6035	2.9149	0.2017	2.9149	a
10:3	0.5738	3.8891	0.2036	3.8769	b

6. Nodal flyby missions to NEAs

The last mission application is related to a nodal flyby mission [21,22] towards a Near Earth Asteroid (NEA) whose population, calculated at mid-January 2011, consists of 7600 bodies.[1] In such a mission scenario, a spacecraft that moves in the ecliptic plane performs a sequence of close encounters with NEAs. To this end, the spacecraft is transferred to a Keplerian orbit in mean motion orbital resonance with the target asteroid's orbit. Accordingly, a flyby occurs in one of the two nodes of the asteroid's heliocentric orbit, that is, when the Sun–spacecraft distance is $r_{☊}$ (ascending node) or $r_{☋}$ (descending node) with

$$r_{☊} = \frac{a_n(1-e_n^2)}{1+e_n\cos\omega_n}, \quad r_{☋} = \frac{a_n(1-e_n^2)}{1+e_n\cos(\pi-\omega_n)} \tag{41}$$

where a_n is the semimajor axis, e_n is the eccentricity, and ω_n is the argument of periapsis of the target asteroid's heliocentric orbit.

The analysis of the problem in the energy plane detects the optimal strategy and provides an estimate of the minimum characteristic acceleration required to perform the transfer phase of the mission. To reduce the problem complexity, the ephemeris constraint is neglected, and a circular parking orbit of radius $r_0 = r_\oplus$ is assumed. In other terms, the problem is now to find the minimum value $\beta_{\min}$ and the jettison distance r_j required to transfer the spacecraft from a circular parking orbit of radius $r_\oplus$ to an elliptic heliocentric orbit of given resonance ratio $q \triangleq T_k/T_n$, where $T_n = 2\pi\sqrt{a_n^3/\mu_\odot}$ is the asteroid's orbital period. For a given pair (q, T_n), the optimal dimensionless

[1] The catalog of NEAs orbital elements is available online at http://newton.dm.unipi.it/neodys/ [retrieved 14 January 2011].

Please cite this article as: G. Mengali, et al., A graphical approach to electric sail mission design with radial thrust, Acta Astronautica (2012), http://dx.doi.org/10.1016/j.actaastro.2012.03.022

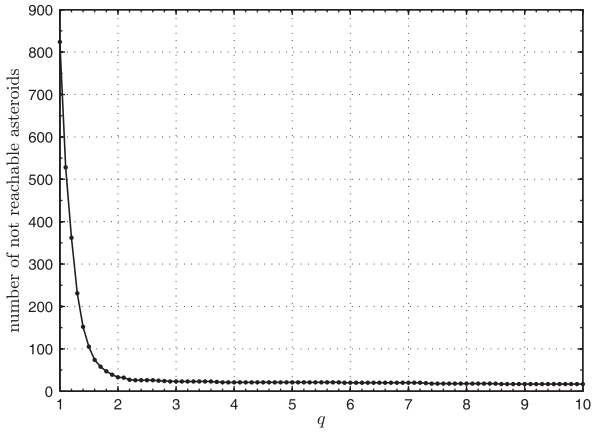

Fig. 17. Number of unreachable asteroids as a function of the resonance ratio $q \geq 1$.

characteristic acceleration $\beta_{\min}$ and the corresponding jettison distance r_j are obtained with the approach described in the previous section.

Note that the constraint on the semilatus rectum states that the transfer is infeasible if $q < T_0/T_n$. Moreover, for a given value of $q > T_0/T_n$, the flyby is impossible if $\{r_{\mathfrak{Q}}, r_{\mathfrak{V}}\} \cap [r_p, r_a] = \{0\}$, where r_p and r_a, that is, the perihelion and aphelion distances of the Keplerian orbit, are given by Eqs. (35) and (36) with $T_k = qT_n$.

The number of unreachable asteroids decreases with the resonance ratio q, as is shown in Fig. 17. For example, when $q=1$ about 824 asteroids (10.8% of the entire population) are not reachable, whereas when $q=2$ the number of "forbidden" asteroids reduces to 33 (0.43% only of the entire population). The horizontal asymptote in Fig. 17 shows that a nodal flyby mission is impossible for a set of 16 NEAs. For these asteroids the value of both $r_{\mathfrak{Q}}$ and $r_{\mathfrak{V}}$ is less than $r_0/2 = 0.5$ AU.

Fig. 18 shows the minimum dimensionless characteristic acceleration $\beta_{\min}$ and the jettison distance r_j as a function of the resonance ratio q for the asteroids population. Note that the cumulative percent in the abscissa of Fig. 18 refers to the actually reachable asteroids for a given value of q, see also Fig. 17.

Fig. 18(a) shows that the required value of $\beta_{\min}$ increases with q and for $q > 3$ nearly all of the asteroids population is reachable with an E-sail of $\beta_{\min} = \beta^\star$. The resonance ratio q is therefore an important parameter for assessing the E-sail capabilities in this mission type. In fact, when $a_\oplus \leq 0.5$ mm/s^2 (or $\beta \leq 0.0843$) the number of reachable asteroids is strongly dependent on the value of q, as is shown in Table 2.

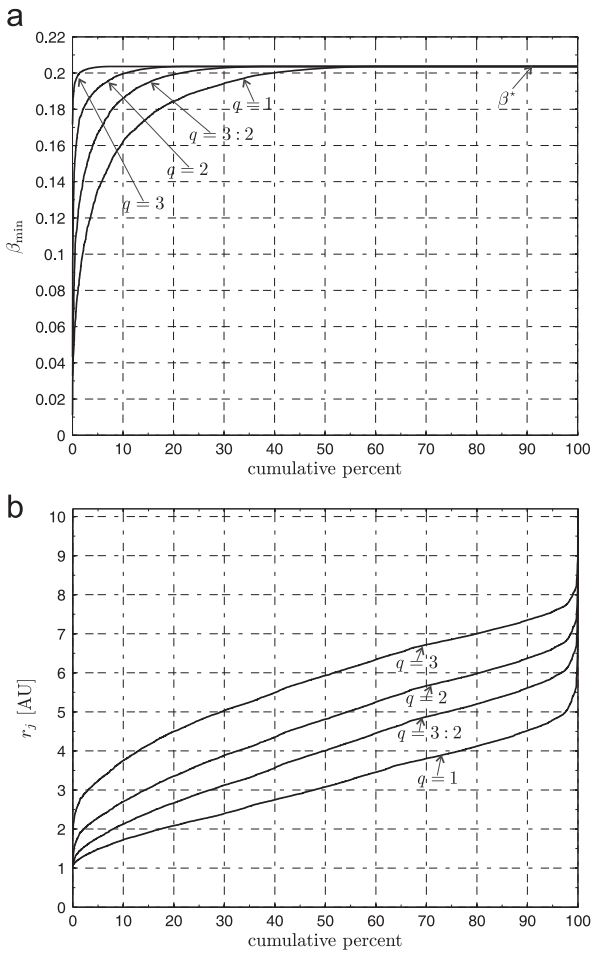

Fig. 18. Optimal performances for a nodal flyby mission towards a NEA, starting from a circular parking orbit of radius $r_0 = r_\oplus$. (a) Dimensionless characteristic acceleration and (b) Jettison distance.

Table 2
Number of reachable NEAs as a function of $a_\oplus$ and q.

Characteristic acceleration	$q=1$	$q=3:2$	$q=2$
$a_\oplus \leq 0.07$ mm/s^2	1	0	0
$a_\oplus \leq 0.2$ mm/s^2	5	2	0
$a_\oplus \leq 0.1$ mm/s^2	2	0	0
$a_\oplus \leq 0.3$ mm/s^2	19	7	1
$a_\oplus \leq 0.4$ mm/s^2	45	15	2
$a_\oplus \leq 0.5$ mm/s^2	88	25	3

7. Conclusions

A new graphical approach for the preliminary mission analysis of an E-sail spacecraft has been illustrated. Assuming that the thrust is always oriented radial with respect to the Sun–spacecraft direction, the space vehicle is subjected to a propulsive, outward, acceleration that varies inversely proportional with the distance from the Sun. The assumption of radial thrust not only is a means to reduce the problem mathematical complexity, but could also be a potentially useful concept from an engineering viewpoint. Indeed, while in principle the E-sail can be slightly inclined and thereby produce an off-radial thrust, maintaining the sail nominal plane orthogonal to the solar wind flow during the whole mission would simplify the design of some spacecraft elements as, for example, thermal and high voltage subsystems. Therefore, it cannot be excluded that a purely radial thrust could be, in practice, an optimal engineering solution, or that if the

Please cite this article as: G. Mengali, et al., A graphical approach to electric sail mission design with radial thrust, Acta Astronautica (2012), http://dx.doi.org/10.1016/j.actaastro.2012.03.022

E-sail nominal plane is inclined, a useful starting point for mission analysis could be provided by the purely radial propulsive acceleration approximation. In this scenario, the spacecraft trajectory is conveniently described in the energy plane, in which the feasible motion is constrained by the potential well concept. With a suitable choice of the independent variables, a new definition of energy plane and potential well has been introduced to obtain a problem solution through a graphical approach. In particular, the main orbital parameters, as the maximum and minimum attainable distance from the Sun, can be calculated by simply intersecting the potential well boundary with a straight line whose slope is proportional to the E-sail characteristic acceleration. As a result, a number of interesting problems involving an E-sail subject to a purely radial thrust can be solved using a semi-analytical approach, without the need to resort to lengthy numerical simulations.

Acknowledgments

This research was financed in part within the European Community's Seventh Framework Programme ([FP7/2007-2013]) under grant agreement number 262733.

References

[1] J.A. Kechichian, Optimal low-thrust transfer using variable bounded thrust, Acta Astronaut. 36 (7) (1995) 357–365, http://dx.doi.org/10.1016/0094-5765(95)00112-3.
[2] G. Mengali, A.A. Quarta, Fuel-optimal, power-limited rendezvous with variable thruster efficiency, J. Guidance Control Dyn. 28 (6) (2005) 1194–1199, http://dx.doi.org/10.2514/1.12480.
[3] M. Otten, C.R. McInnes, Near minimum-time trajectories for solar sails, J. Guidance Control Dyn. 24 (3) (2001) 632–634, http://dx.doi.org/10.2514/2.4758.
[4] G. Mengali, A.A. Quarta, Optimal control laws for axially symmetric solar sails, J. Spacecr. Rockets 42 (6) (2005) 1130–1133, http://dx.doi.org/10.2514/1.17102.
[5] P. Janhunen, The electrical sail—a new propulsion method which may enable fast missions to the outer solar system, J. Br. Interplanet. Soc. 61 (2008) 322–325.
[6] G. Mengali, A.A. Quarta, Non-Keplerian orbits for electric sails, Celestial Mech. Dyn. Astron. 105 (1–3) (2009) 179–195, http://dx.doi.org/10.1007/s10569-009-9200-y.
[7] G. Mengali, A.A. Quarta, P. Janhunen, Electric sail performance analysis, J. Spacecr. Rockets 45 (1) (2008) 122–129, http://dx.doi.org/10.2514/1.31769.
[8] G. Mengali, A.A. Quarta, P. Janhunen, Considerations of electric sailcraft trajectory design, J. Br. Interplanet. Soc. 61 (2008) 326–329.
[9] A.A. Quarta, G. Mengali, P. Janhunen, Optimal interplanetary rendezvous combining electric sail and high thrust propulsion system, Acta Astronaut. 68 (5–6) (2011) 603–621, http://dx.doi.org/10.1016/j.actaastro.2010.01.024.
[10] A.A. Quarta, G. Mengali, Electric sail missions to potentially hazardous asteroids, Acta Astronaut. 66 (9–10) (2010) 1506–1519, http://dx.doi.org/10.1016/j.actaastro.2009.11.021.
[11] H.S. Tsien, Take-off from satellite orbit, J. Am. Rocket Soc. 23 (4) (1953) 233–236.
[12] G. Mengali, A.A. Quarta, Escape from elliptic orbit using constant radial thrust, J. Guidance Control Dyn. 32 (3) (2009) 1018–1022, http://dx.doi.org/10.2514/1.43382.
[13] J.E. Prussing, V.L. Coverstone, Constant radial thrust acceleration redux, J. Guidance Control Dyn. 21 (3) (1998) 516–518, http://dx.doi.org/10.2514/2.7609.
[14] P. Janhunen, Electric sail for spacecraft propulsion, J. Propul. Power 20 (4) (2004) 763–764, http://dx.doi.org/10.2514/1.8580.
[15] P. Janhunen, A. Sandroos, Simulation study of solar wind push on a charged wire: basis of solar wind electric sail propulsion, Ann. Geophys. 25 (3) (2007) 755–767, http://dx.doi.org/10.5194/angeo-25-755-2007.
[16] P. Janhunen, The electric solar wind sail status report, in: European Planetary Science Congress 2010, Rome, Italy, vol. 5, 2010, Paper EPSC 2010-297.
[17] C.R. McInnes, Solar Sailing: Technology, Dynamics and Mission Applications, Springer-Praxis Series in Space Science and Technology, Springer-Verlag, Berlin, 1999, pp. 46–54, ISBN: 3-540-21062-8.
[18] J.L. Wright, Space Sailing, Gordon and Breach Science Publisher, Berlin, 1992, pp. 223–226, ISBN: 2-881-24842-X.
[19] R.H. Battin, An Introduction to the Mathematics and Methods of Astrodynamics, revised ed., AIAA Education Series, AIAA, New York, 1999, pp. 408–415, ISBN: 1-563-47342-9.
[20] R.J. McKay, M. Macdonald, J. Biggs, C.R. McInnes, Survey of highly non-Keplerian orbits with low-thrust propulsion, J. Guidance Control Dyn. 34 (3) (2011) 645–666, http://dx.doi.org/10.2514/1.52133.
[21] E. Perozzi, L. Casalino, G. Colasurdo, A. Rossi, G.B. Valsecchi, Resonant fly-by missions to near earth asteroids, Celestial Mech. Dyn. Astron. 83 (1–4) (2002) 49–62, http://dx.doi.org/10.1023/A:1020122511548.
[22] R.P. Binzel, E. Perozzi, A.S. Rivkin, A. Rossi, A.W. Harris, S.J. Bus, G.B. Valsecchi, S.M. Slivan, Dynamical and compositional assessment of near-Earth object mission targets, Meteorit. Planet. Sci. 39 (3) (2004) 351–366, http://dx.doi.org/10.1111/j.1945-5100.2004.tb00098.x.

Please cite this article as: G. Mengali, et al., A graphical approach to electric sail mission design with radial thrust, Acta Astronautica (2012), http://dx.doi.org/10.1016/j.actaastro.2012.03.022